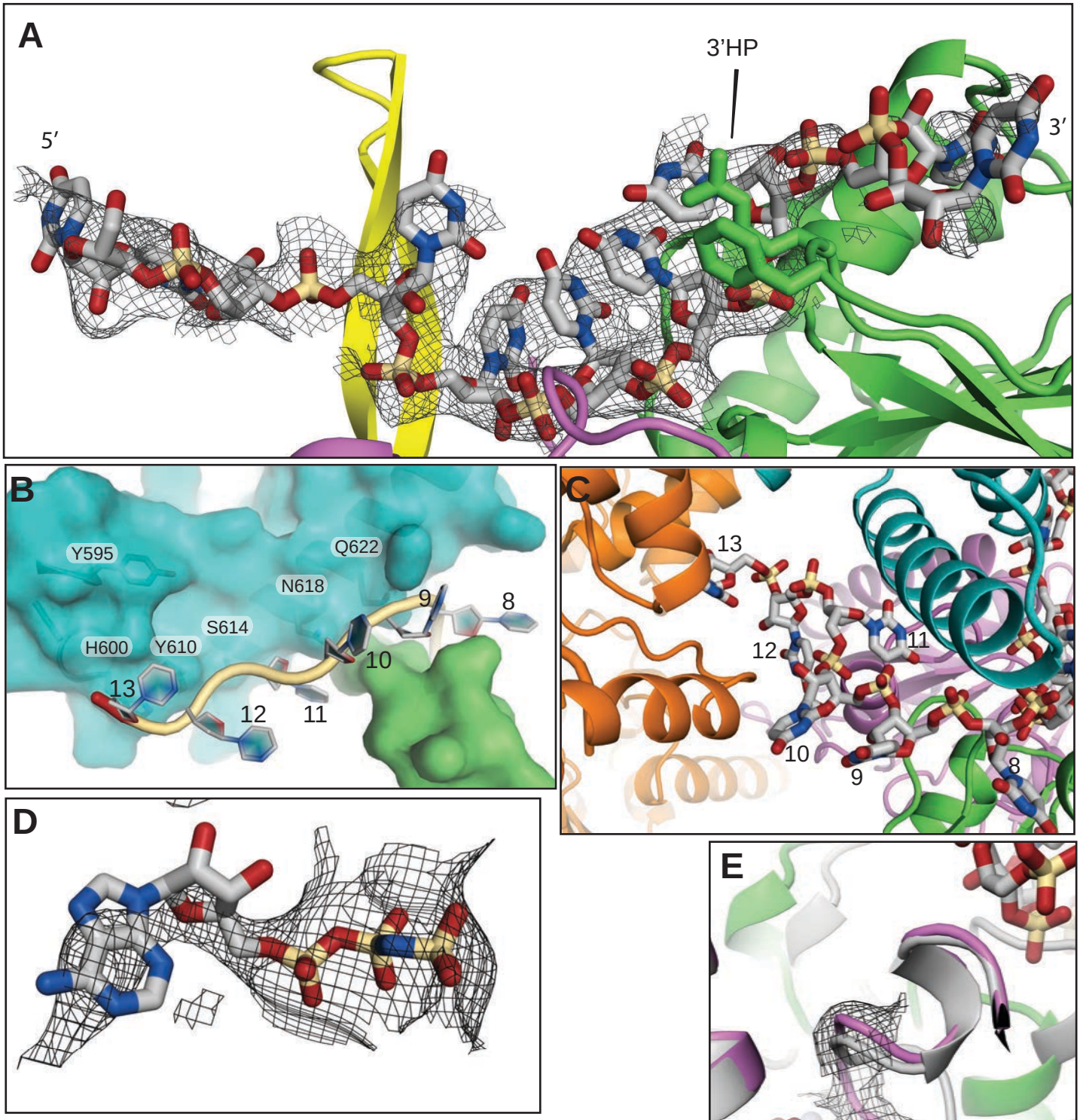

SUPPLEMENTAL FIGURE 1. Differences between the RNA in complex A and B in the asymmetric unit and omit maps of RNA, ADPNP, and motif Va.
(*A*) Nine bases can be resolved in complex A with continuous electron density for bases 1-7, while base 8 has intermediate density and base 9 has poor density. A $2mF_o$-DF_c electron density omit map surrounding the RNA in complex A is shown, non-averaged and contoured at 0.8 σ. The RecA1 and RecA2 domains including the 5'HP are shown. (*B*) Cartoon representation of RNA and surface representation of the ratchet domain, demonstrating proximity of indicated nucleotides. (*C*) The additional four nucleotides at the 3' end of the RNA in complex B may be stabilized by crystal packing. A symmetry-related molecule is shown in orange. (*D*) A $2mF_o$-DF_c electron density omit map surrounding the ADPNP in complex B is shown, averaged and contoured at 1.0 σ. (*E*) A $2mF_o$-DF_c electron density omit map surrounding motiv Va in complex B is shown, averaged and contoured at 1.0 σ. The Prp43p-ADP structure (PDB 3KX2) is shown in grey, with RecA1 superimposed, validating the different conformations of motiv Va between the two structures.

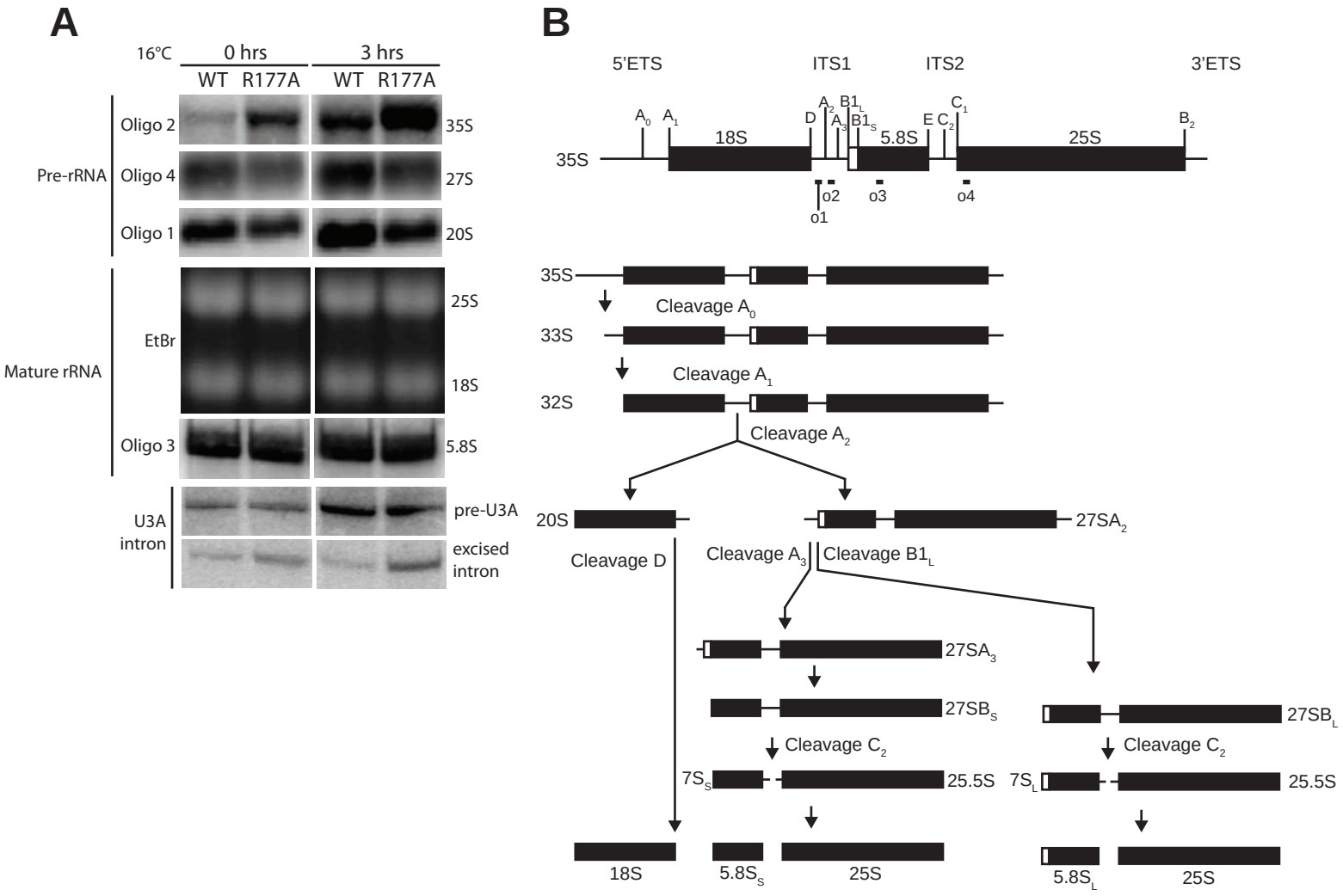

SUPPLEMENTAL FIGURE 2. The Prp43p-R177A mutant accumulates 35S pre-rRNA and excised intron after incubation at a cold, non-permissive temperature.

(*A*) Northern analysis of steady-state levels of pre- and mature-ribosomal RNA species and pre-U3A and its excised intron. RNA was extracted from WT (yJPS568) or Prp43p-R177A (yJPS1579) cells cultured at 30 °C or also shifted to 16 °C for 3 hrs. The probes indicated on the left were used for northern analysis of agarose gels (top 8 panels) or acrylamide gels (bottom two panels); for oligo sequences, see Supplemental Table 2; "EtBr" indicates ethidium bromide used to stain mature rRNAs separated on equivalent agarose gels. The pre- and mature-rRNAs and U3A species visualized in each panel are indicated to the right. (*B*) Schematic representation of the 35S pre-rRNA showing endonucleolytic cleavage sites as well as the targets of oligos used for the northern blotting (top) and the pre-ribosomal RNA processing pathway in *S. cerevisiae* is depicted (bottom).

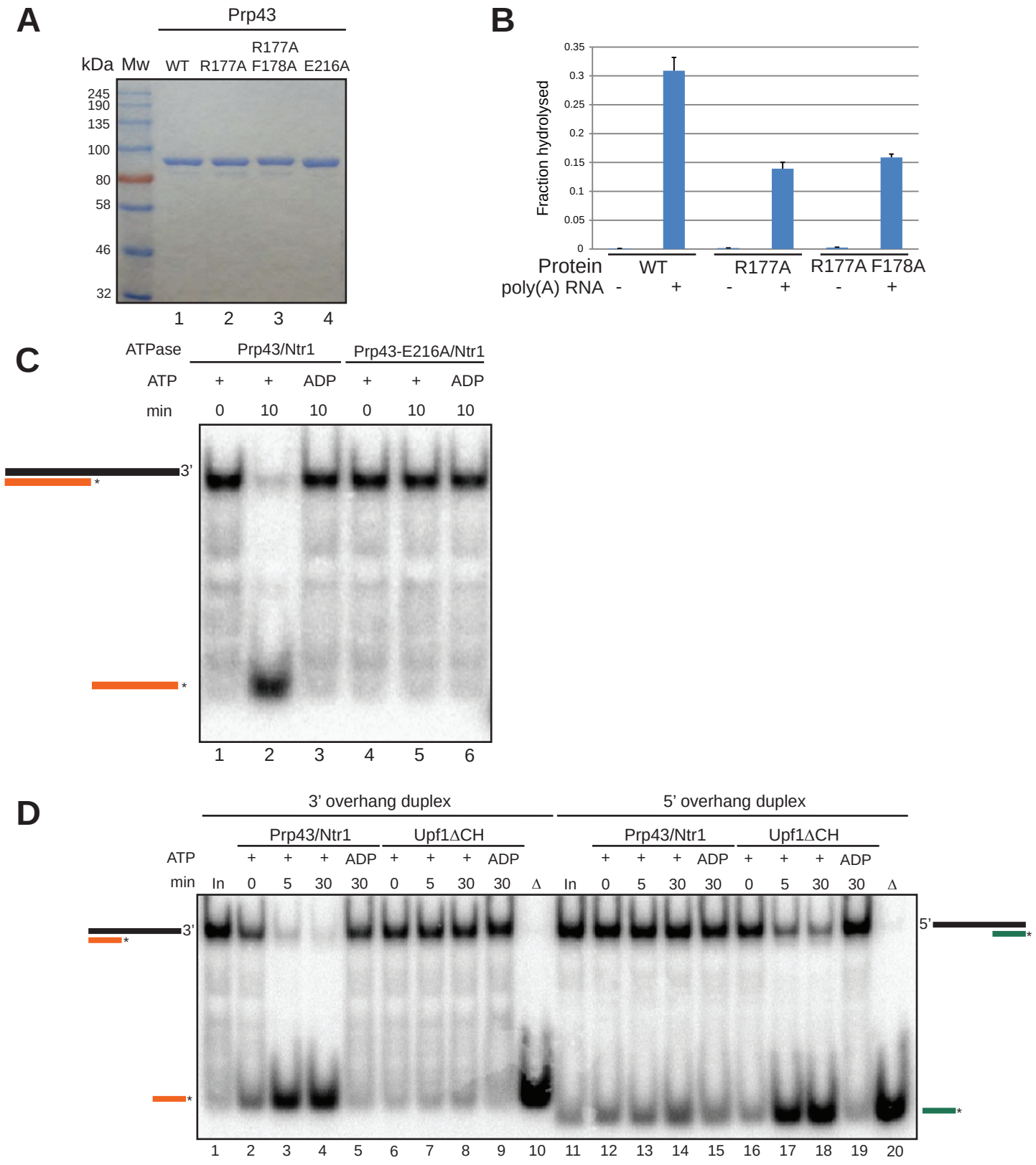

SUPPLEMENTAL FIGURE 3. Expression, unwinding and ATPase assays show that the Prp43p-E216A mutant is defective in unwinding and that WT Prp43p displays 3′-5′ directionality.
(*A*) SDS-PAGE analysis of the purified Prp43p proteins (1 μg of each). (*B*) Quantitation of ATPase activity of Prp43 and variants assayed by TLC as in Figure 5D; error bars, s.d (n=3). (*C*) Unwinding assay as in Figure 5 comparing WT Prp43p with Prp43p-E216A, which is mutated in the Walker B, DEAH-box motif II. (*D*) Unwinding of a 16 bp RNA/DNA duplex with either a 3′ or 5′, unstructured 44 nt RNA overhang was assayed in the presence of either Prp43p/Ntr1 or Upf1ΔCH. The substrate input (In) was analyzed in parallel. RNA is black; DNA, red or green; asterisk indicates radiolabel. Heat denaturation of the duplex (Δ) was used as a positive control for unwinding.

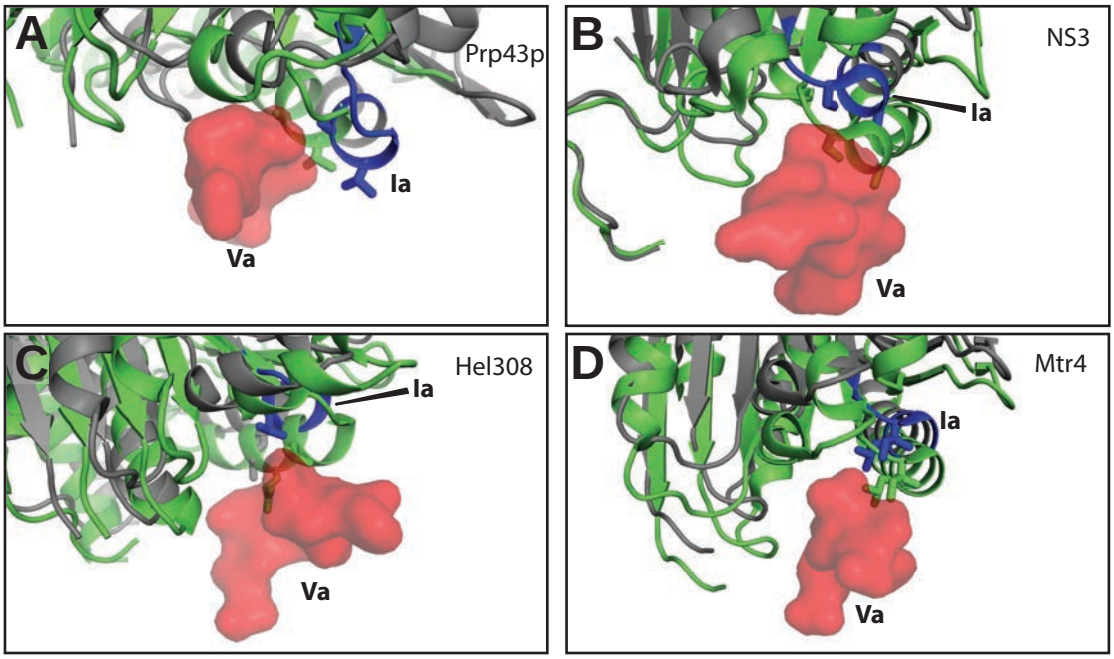

SUPPLEMENTAL FIGURE 4. The configuration of the dynamic motif Va is generally in a position to stabilize the open conformation. (*A-D*) The conformation of motif Va in the open, ATP-free state is shown as a surface representation (transparent red) illustrating how the motif would sterically clash with motif Ia of RecA1 in the closed, ATP-bound state. RecA1 and motif Ia are shown in an open (grey or blue, respectively) or closed (green) state; RecA1 in each case was positioned by superimposing RecA2 of the open and closed states (not shown). For Prp43p (*A*), the open state corresponds to the ADP structure (PDB 3KX2), and the closed state corresponds to the RNA- and ADPPNP-bound structure. For NS3 (*B*), the open state corresponds to an RNA bound, nucleotide-free NS3 structure (PDB 3O8C) and the closed state corresponds to an RNA- bound, ADP-BeF_3 –bound NS3 structure (PDB 3O8R). For Hel308 (*C*), the open state corresponds to the nucleotide-free structure (PDB 2P6R); because there is no Hel308 structure of the closed state, this state was modeled by separating the two RecA domains of the open state and superimposing each on the corresponding RecA domains of the RNA-bound, ADP-BeF_3–bound NS3 structure (PDB 3O8R). For Mtr4 (*D*), the open state corresponds to the nucleotide-free structure (PDB 2XGJ); because there is no Mtr4 structure of the closed state, this state was modeled as in *C*.

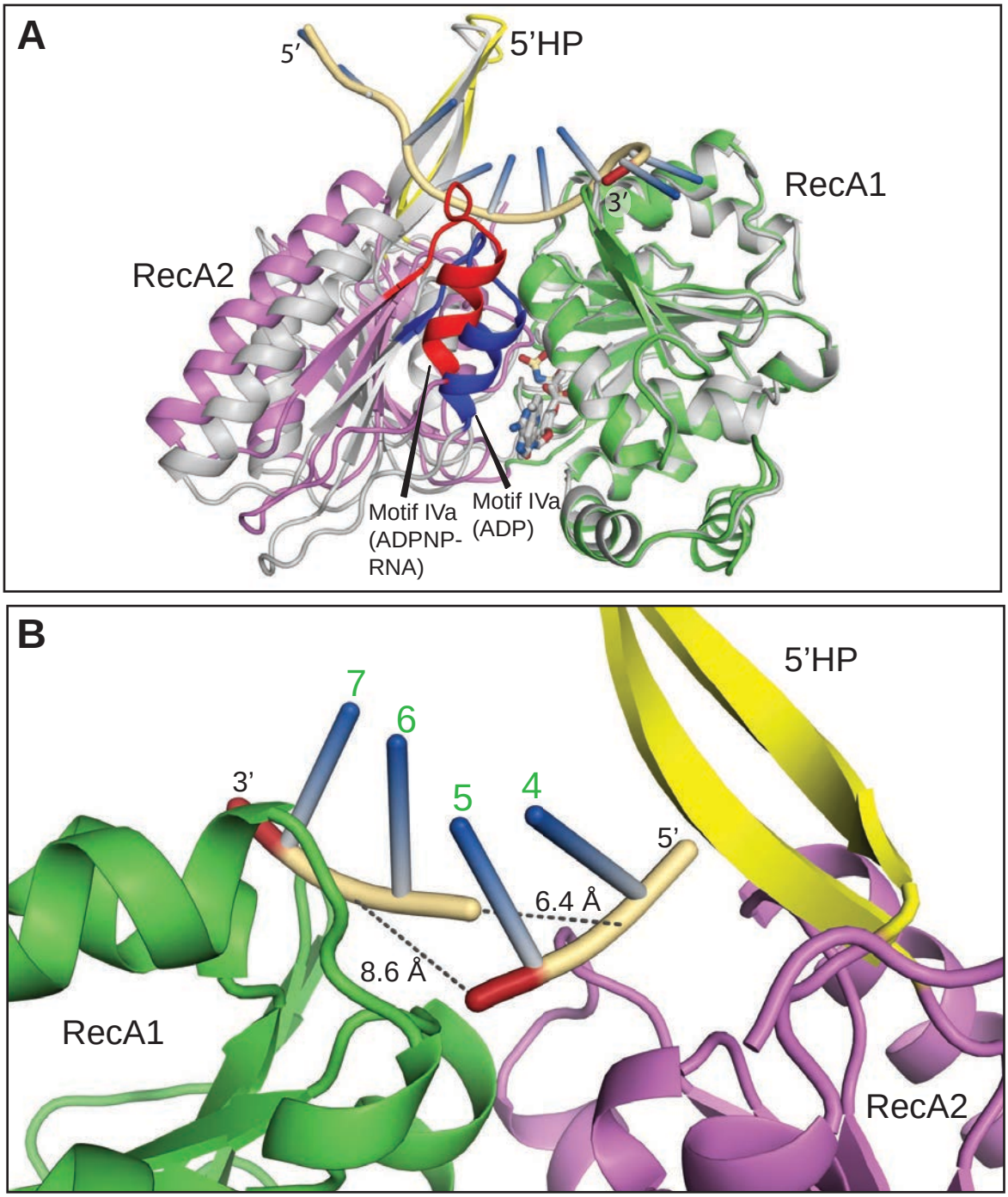

SUPPLEMENTAL FIGURE 5. Rhe RecA domains in the ADP-Prp43p structure are not in a conformation that can bind RNA through canonical motifs.

(*A*) Comparison of the RecA domains of Prp43p in the ADP-bound (grey) and the ADPNP-RNA-bound (colored) states, with the RecA1 domains (green) superimposed. Motif IVa is indicated and colored separately in the ADP-bound (blue) and the RNA-ADPNP-bound (red) states. (*B*) The RecA1 and RecA2 domains, along with the two nucleotides bound to each RecA domain, were separately extracted from the RNA- and ADPNP-bound Prp43p structure and then individually superimposed on the Prp43p-ADP structure. The overlay reveals that a 3 nucleotide RNA strand could not be bound in the ADP (only) configuration through canonical interactions. For example, with the RecA2-RNA interaction fixed, as dictated by the compaction model, upon ATP hydrolysis, residue 6 would need to translocate and replace residue 7; however, this leads to an 8.6 Å separation of atoms that should be covalently linked. Alternatively, RecA2 could remain associated with only residue 4, requiring that residues 5 and 6 translocate and replace residues 6 and 7, respectively; however, this leads to a 6.4 Å separation of residues that should be covalently attached. The RNA is displayed as cartoon; the lengths reflect distances from a phosphate to a 3′ oxygen.

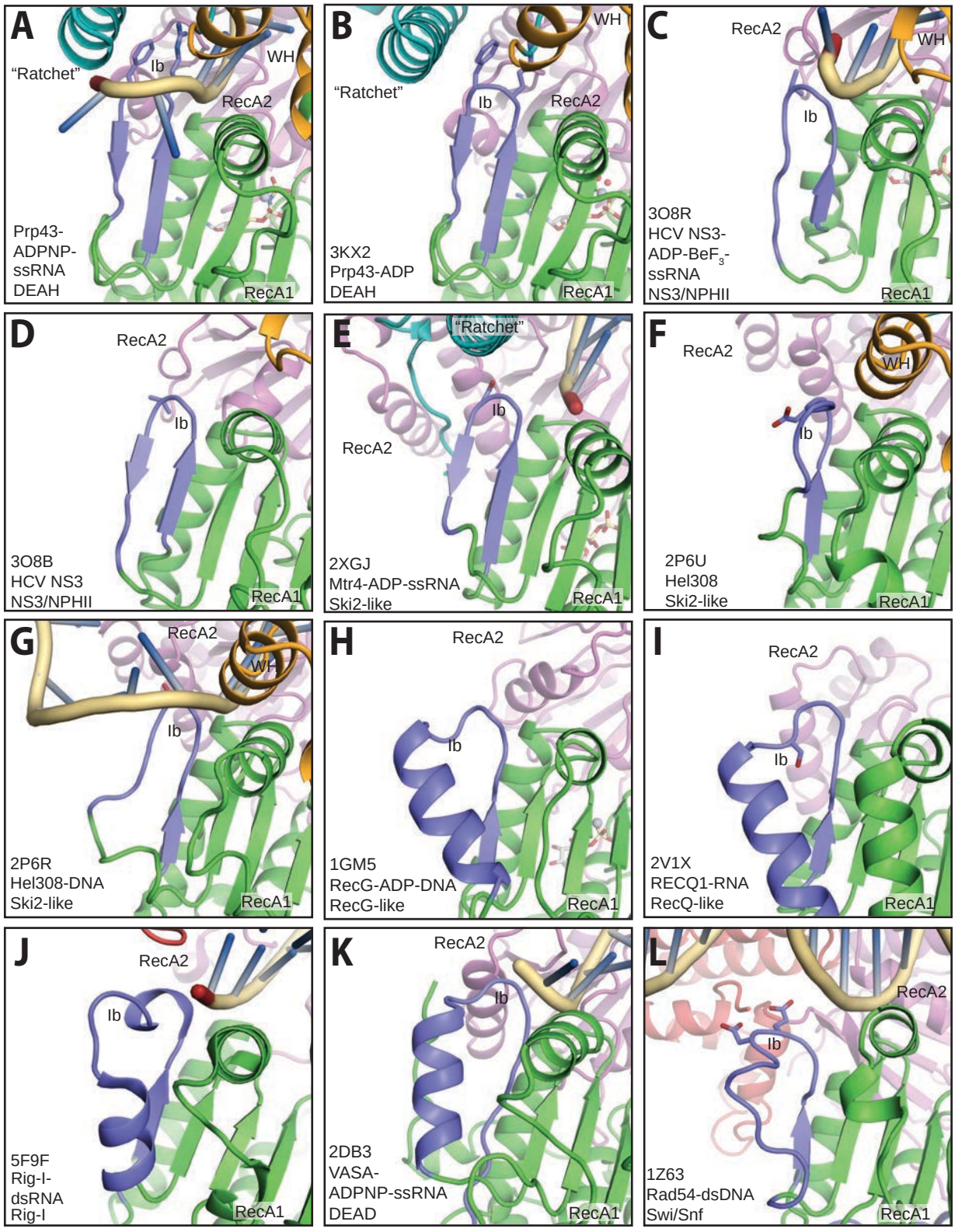

SUPPLEMENTAL FIGURE 6. Variation in the conformations of motif Ib across families of superfamily 2 of nucleic acid-dependent ATPases.

Conformations of motif Ib are shown for the following families: DEAH/RHA (*A-B*), NS3/NPHII (*C-D*), Ski2-like (*E-G*), RecG-like (*H*), RecQ-like (*I*), Rig-I (*J*), DEAD (*K*), and Swi/Snf (*L*). Motif Ib is colored blue; otherwise, domains and nucleic acid are shown as in Figure 1. The RCSB PDB entry code, protein and ligand name, and helicase family name of each structure is annotated.

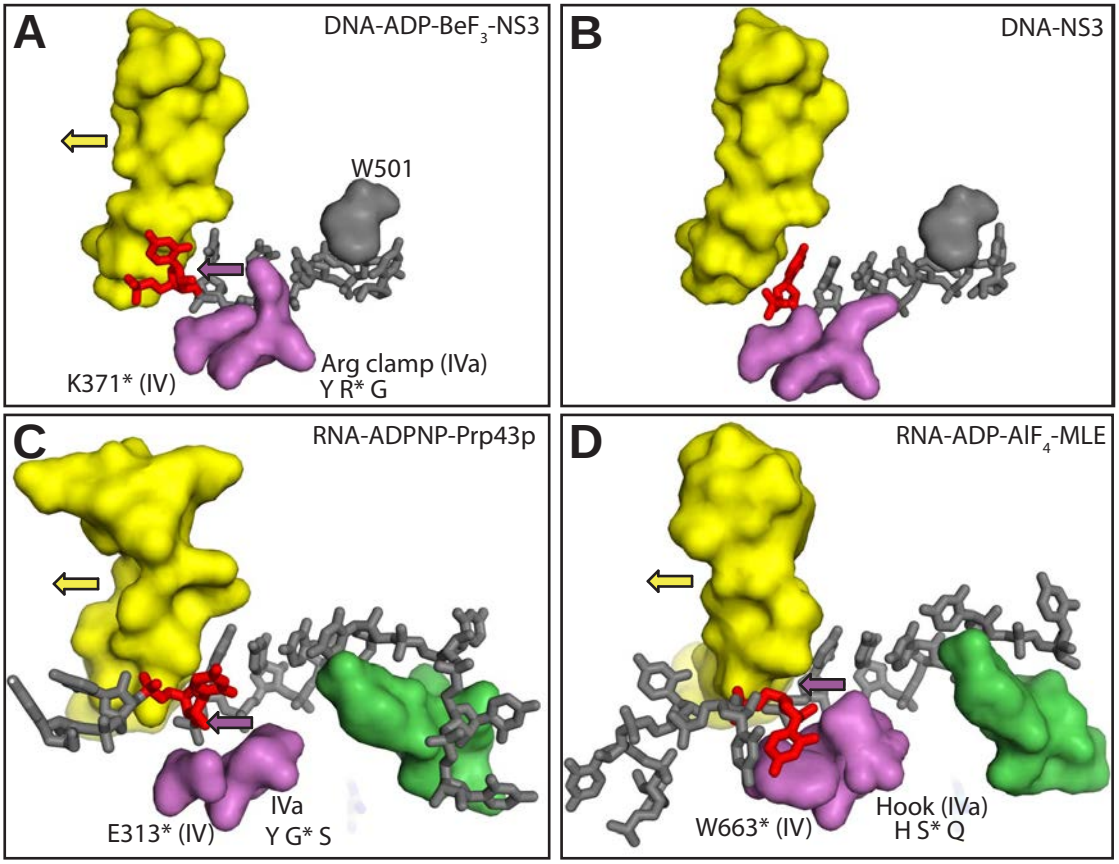

SUPPLEMENTAL FIGURE 7. The motifs IV and IVa are in position to displace the incoming nucleotide to promote its incorporation into the stack.

(*A-D*) During the opening and closing of the RecA domains during the ATP cycle, the 5′HP can more readily move in the 5′ direction, which is unobstructed, than in the 3′ direction, which is blocked by the stack, potentially favoring 3′ to 5′ directionality. By moving in the 5′ direction, the 5′HP would create space for an additional base in the stack and our structure suggests that the capture of an additional base may be facilitated by motifs IV and IVa. Specifically, movement of RecA2 in the 5′ direction would result in steric clashes of motifs IV and IVa with the incoming base, which we propose thereby induces displacement of this base into the stack. The position of motifs IV and IVa, relative to the incoming residue, for NS3 (*A-B*; PDB 3KQH and 3KQU), Prp43p (*C*; PDB 3KX2), and MLE (*D*; PDB 5AOR) is indicated. The arrows indicate the direction of demonstrated (*A-B*) or anticipated (*C-D*) movement for the motifs after ATP hydrolysis, according to the expansion model (Figure 6A). Although the identity of the IV and IVa residues are not conserved between Prp43p, MLE and NS3, conservation is not required for a steric role of motif IVa in displacing the incoming nucleotide. The substrate is shown as sticks colored grey except for the nucleotide (red) that is about to enter the stack (*A,C-D*) or has entered the stack (*B*). Motifs IV and IVa are purple; the 5′HP, yellow; the 3′HP, green, and W501 from NS3, grey; and all are shown as surface representations; the residues of motifs IV and IVa represented are indicated, with the asterisk denoting the residues that interact directly with RNA through their backbone.

Prp43p	**Arg150 MC**	**Arg177 MC**[$]	**Thr192 SC**	**Glu313 MC**	**Gly346 MC**	**Thr376 SC**	**Lys398 SC**
Motif	Ia	Ib	Ic	IV	IVa	V	5'HP
DEAD (VASA)	Yes (R328)	Yes (G354)&	Yes (T375)	Yes (K499)	Yes (G521)	Yes (T546)	N/A
NS3/NPH-II	Yes (V232)	Yes (G255)#	Yes (T269)	Yes (K371)	Yes (R393)	Yes (T411)	No (V432)
MLE (DEAH/RHA)	Yes (R443)	Yes (R470)	Yes (T486)	Yes (W663)	Yes (S692)	Yes (T717)	Yes (R739)
Mtr4 (Ski2-like)	Yes (K202)	(G224)*	(T238)*	Yes (K416)	Yes (S477)	Yes (T502)	No (W524)
Hel308 (Ski2-like)	Yes (R78)	Yes (G103)	Yes (T121)	Yes (R252)	Yes (A304)	Yes (T329)	No (F351)
Rig-1	Yes (I300)	Yes (G326)	Yes (T347)	Yes (R637)	(T671)**	Yes (T697)	N/A
SF1	Yes (R,N,G,H)	N/A	Yes	Yes (N,E,R)	N/A	Yes	N/A

SUPPLEMENTAL TABLE S1. Overview of conserved interactions with RNA/DNA of SF1 and SF2 helicases

$ The distance for the backbone amide interaction between R177 and the RNA phosphate backbone is slightly longer than would be expected for such an interaction, which probably due to the resolution of our structure as the equivalent interaction is present in the 2.1Å structure of the DEAH/RHA ATPase MLE (PDB 5AOR), & G354 is the first G of the conserved GG motif (Ib) also observed for the remaining SF2 members except for DEAH/RHA members that contain an Arg, # hydrogen bond is present in the apo-RNA and DNA structures (PDB 3KQH and 3O8C) and in the ADP-BeFx-DNA structure (PDB 3O8R) but bond not in ADP-BeFx-RNA structure (PDB 3KQU), * RNA too short to observe potential interaction (PDB 2XGJ), ** Several RigI structures are unstructured in this region; however, while PDB 5F9F is complete T671 is not positioned so it can interact with RNA. Abbreviations: N/A, not applicable. MC, main chain interaction. SC, side chain interaction.

The following structures were used for the alignment: SF2 members; (VASA; PDP 2DB3 (Sengoku et al. 2006)), (Hel308; PDB 2P6R (Büttner et al. 2007)), (Mtr4; PDB 2XGJ (Weir et al. 2010)), (RigI; PDB 5F9F (Devarkar et al. 2016)), (MLE; PDB 5AOR (Prabu et al. 2015)), (NS3; PDB 3KQU (Appleby et al. 2011), 3KQH (Appleby et al. 2011), 3O8C (Gu and Rice 2010), 3O8R (Gu and Rice 2010)) and SF1 members; (Dda; PDB 3UPU (He et al. 2012)), (PcrA; PDB 3PJR (Velankar et al. 1999)), (Upf1; PDB 2XZL (Chakrabarti et al. 2011)), (RecD2; PDB 3GPL (Saikrishnan et al. 2009)).

Unwinding.

Oligonucleotide	Sequence (5′ to 3′)
RNA-1-3′overhang 60 nts	GGCACCAACACAAAACACAUCUACACUCAACAAUCACUUUUUAUACAACACUUCUUCUCU[#]
DNA-1	GGGAATTTAATACGACTCACTATAGGCACCAACACAAAACACATCTACACTCAACAATCACTTTTTATACAACACTTCTTCTCT
T7-promoter rev	GGGAATTTAATACGACTCACTATAGGCA
DNA-1 fwd	AGAGAAGAAGTGTTGTATAAAAAGTGATTGTTG[*]
RNA-2-5′overhang 60 nts	GGCAAUCACUUUUUAUACAACACUUCUUCUCUGGCACCAACACAAAACACAUCUACACUC
DNA-2	GGGAATTTAATACGACTCACTATAGGCAATCACTTTTTATACAACACTTCTTCTCTGGCACCAACACAAAACACATCTACACTC
DNA-2 fwd	GAGTGTAGATGTGTTTTGTGTTGGTG[*]
RNA3-3′overhang 48 nts	GGCACCAACACAAAACACAUCUACACUCAACAAUCACUUUUUAUACAA
DNA-UW1 16 nts	GTTTTGTGTTGGTGCC
DNA-UW2 16 nts	GAGTGTAGATGTGTTT
DNA-UW3 21 nts	GATGTGTTTTGTGTTGGTGCC

[#] This RNA strand corresponds to the first 60 nts of an unstructured long RNA ssRNA-76(Nallagatla et al. 2007)

[*] The first two residues are 2-O-methylated to reduce nontemplated nucleotide addition during T7 RNA transcription(Kao et al. 1999)

Northern blotting. The target of the oligos is outlined in Supplemental Figure 4.

Oligonucleotide	Sequence (5′ to 3′)
o1	GCTCTTTGCTCTTGCC
o2	ATGAAAACTCCACAGTG
o3	ATTCACGGAATTCTGCAATTCAC
o4	GCCCGTTCCCTTGGCTGTG
U3A intron	CAAAAGCTGCTGCAATGG

SUPPLEMENTAL TABLE S2 Oligos used in this study.

Plasmid	Description	Reference
pJPS261	pRS316-*PRP43-URA3*	(Leeds et al. 2006)
pJPS298	pRS315-*PRP43-LEU2*	(Leeds et al. 2006)
pJPS632	pET15b-*HIS$_6$-PRP43*	(Mayas et al. 2006)
pJPS2657	pET52b-*HIS$_6$-TEV-PRP43*	(He et al. 2010)
pHE205	pET28a-CBP-UPF1ΔCH	(Fiorini et al. 2012)
pJPS2689	pRS315-*PRP43-R177A-LEU2*	this study
pJPS2690	pRS315-*PRP43-F178A-LEU2*	this study
pJPS2691	pRS315-*PRP43-R177A-F178A-LEU2*	this study
pJPS2692	pRS315-*PRP43-P521A-LEU2*	this study
pJPS2693	pRS315-*PRP43-R177A-P521A-LEU2*	this study
pJPS2694	pRS315-*PRP43-K398A-LEU2*	this study
pJPS2695	pRS315-*PRP43-R177A-K398-LEU2*	this study
pJPS2696	pRS315-*PRP43-R177K-LEU2*	this study
pJPS2697	pRS315-*PRP43-F178H-LEU2*	this study
pJPS2698	pRS315-*PRP43-Y610A-LEU2*	this study
pJPS2699	pRS315-*PRP43-R611A-LEU2*	this study
pJPS2700	pRS315-*PRP43-Q622A-LEU2*	this study

SUPPLEMENTAL TABLE S3 Plasmids used in this study.

SUPPLEMENTAL REFERENCES

Appleby TC, Anderson R, Fedorova O, Pyle AM, Wang R, Liu X, Brendza KM, Somoza JR. 2011. Visualizing ATP-dependent RNA translocation by the NS3 helicase from HCV. *J Mol Biol* **405**: 1139–53.

Büttner K, Nehring S, Hopfner KP. 2007. Structural basis for DNA duplex separation by a superfamily-2 helicase. *Nat Struct Mol Biol* **14**: 647–652.

Chakrabarti S, Jayachandran U, Bonneau F, Fiorini F, Basquin C, Domcke S, Le Hir H, Conti E. 2011. Molecular Mechanisms for the RNA-Dependent ATPase Activity of Upf1 and Its Regulation by Upf2. *Mol Cell* **41**: 693–703.

Devarkar SC, Wang C, Miller MT, Ramanathan A, Jiang F, Khan AG, Patel SS, Marcotrigiano J. 2016. Structural basis for m7G recognition and 2'-O-methyl discrimination in capped RNAs by the innate immune receptor RIG-I. *Proc Natl Acad Sci U S A* **113**: 596–601.

Fiorini F, Bonneau F, Hir H Le. 2012. Biochemical characterization of the RNA helicase UPF1 involved in nonsense-mediated mRNA decay. *Methods Enzym* **511**: 255–274.

Gu M, Rice CM. 2010. Three conformational snapshots of the hepatitis C virus NS3 helicase reveal a ratchet translocation mechanism. *Proc Natl Acad Sci U S A* **107**: 521–8.

He X, Byrd AK, Yun MK, Pemble CW th, Harrison D, Yeruva L, Dahl C, Kreuzer KN, Raney KD, White SW. 2012. The T4 phage SF1B helicase Dda is structurally optimized to perform DNA strand separation. *Structure* **20**: 1189–1200.

He Y, Andersen GR, Nielsen KH. 2010. Structural basis for the function of DEAH helicases. *EMBO Rep* **11**: 180–186.

Kao C, Zheng M, Rüdisser S. 1999. A simple and efficient method to reduce nontemplated

nucleotide addition at the 3 terminus of RNAs transcribed by T7 RNA polymerase. *RNA* **5**: 1268–72.

Leeds N, Small E, Hiley SL, Hughes TR, Staley JP. 2006. The splicing factor Prp43p, a DEAH box ATPase, functions in ribosome biogenesis. *Mol Cell Biol* **26**: 513–522.

Mayas RM, Maita H, Staley JP. 2006. Exon ligation is proofread by the DExD/H-box ATPase Prp22p. *Nat Struct Mol Biol* **13**: 482–90.

Nallagatla SR, Hwang J, Toroney R, Zheng X, Cameron CE, Bevilacqua PC. 2007. 5'-triphosphate-dependent activation of PKR by RNAs with short stem-loops. *Science* **318**: 1455–1458.

Prabu JR, Müller M, Thomae AW, Schüssler S, Bonneau F, Becker PB, Conti E. 2015. Structure of the RNA helicase MLE reveals the molecular mechanisms for uridine specificity and RNA-ATP coupling. *Mol Cell* **60**: 487–499.

Saikrishnan K, Powell B, Cook NJ, Webb MR, Wigley DB. 2009. Mechanistic basis of 5'-3' translocation in SF1B helicases. *Cell* **137**: 849–59.

Sengoku T, Nureki O, Nakamura A, Kobayashi S, Yokoyama S. 2006. Structural basis for RNA unwinding by the DEAD-box protein Drosophila Vasa. *Cell* **125**: 287–300.

Velankar SS, Soultanas P, Dillingham MS, Subramanya HS, Wigley DB. 1999. Crystal structures of complexes of PcrA DNA helicase with a DNA substrate indicate an inchworm mechanism. *Cell* **97**: 75–84.

Weir JR, Bonneau F, Hentschel J, Conti E. 2010. Structural analysis reveals the characteristic features of Mtr4, a DExH helicase involved in nuclear RNA processing and surveillance. *Proc Natl Acad Sci U S A* **107**: 12139–44.